Absorption Cross Section and Interfacial Thermal Conductance from an Individual Optically Excited Single-Walled Carbon Nanotube

Dan Wang,[†] Michael T. Carlson, and Hugh H. Richardson*

Department of Chemistry and Biochemistry, Ohio University, Athens, Ohio 45701, United States. [†]Present address: Center for Electrochemical Engineering Research, Department of Chemical and Biomolecular Engineering, Ohio University.

ABSTRACT The heat generation and dissipation of an individual optically excited metallic single-walled carbon nanotube is characterized using a thermal sensor thin film of $Al_{0.94}Ga_{0.06}N$ embedded with Er^{3+}. The absorption cross section from an individual SWCNT excited at 532 nm is revealed from the steady-state temperature of the thermal sensor film. A maximum temperature of 4.3 K is observed when the SWCNT is excited with parallel polarization and an average intensity of 7×10^{10} W/m^2. From this temperature measurement, we determine an absorption cross section for the SWCNT of 9.4×10^{-17} m$^2/\mu$m using parallel polarization and 2.4×10^{-17} m$^2/\mu$m for perpendicular polarization. We establish a temperature difference between the SWCNT and the substrate of 315 K by converting the G band shift of the SWCNT into the local SWCNT temperature and scaling the measured film temperature to the local non-resolution-limited temperature rise. From the temperature difference and heat flux, we deduce a value of 6.6 MW/m$^2 \cdot$K for the thermal interfacial conductance of a SWCNT sitting on a thin film of amorphous $Al_{0.94}Ga_{0.06}N$.

KEYWORDS: heat generation · single-walled carbon nanotubes · absorption cross section · interfacial thermal conductance

Single-wall carbon nanotubes (SWCNTs) exhibit excellent electrical,[1] thermal,[2−5] mechanical,[6] and optical properties[7−10] due to their unique one-dimensional all-carbon structure and have been demonstrated as an important starting material for many novel nanodevices. The superb thermal conductivities and stability offer carbon nanotubes great potential in applications ranging from thermal interface materials and electronics to sensors.[11−14] Moreover, the processes of optical irradiation of SWCNTs can generate heat and be used in the fields of cancer biology, nanomedicine, and phonon waveguides.[15−17]

Thermal management and optical characterization at the nanoscale is important for the applications where heat accumulation within the nanodevice causes an increase in temperature. The interfacial boundary resistance is also an important consideration when determining heat generation and dissipation from composite materials made from carbon nanotubes.[18−21] However, the characterization of heat generation, local temperature, interfacial thermal conductance, and optical absorption cross section of individual SWCNTs remains a difficult measurement.[22−24] Recently, we developed a novel optical thermal sensor to image the temperature profile of optically excited nanoparticles.[25] In this paper, we use a thin film thermometer based on Er^{3+} photoluminescence to measure the nanoscale temperature of the film when a metallic SWCNT is excited with 532 nm light. Raman spectra are collected simultaneously and used to characterize the carbon nanotube structure and temperature. From our temperature measurement, we determine the absorption cross section of an individual SWCNT and the interfacial thermal resistance between the SWCNT and the thin film thermometer.

RESULTS

Optical Characterization of SWCNTs. The optical characterization of the SWCNT immobilized on the AlN:Er^{3+} surface has been described previously,[26] with only the major points of the characterization given here. The Raman image of a SWCNT is shown in Figure 1A. The SWCNT bands are located at 1320 cm^{-1} (D band), 1560 cm^{-1} (G band), and 2650 cm^{-1} (G′ band). The radial breathing mode is obscured by the photoluminescence peaks from Er^{3+} ions excited in the underlying thin film. The inset in Figure 1A shows one spectral component from SIMPLISMA[27] of the low-energy region in the SWCNT Raman spectrum.[26]

The band shape of the G band is analyzed by peak fitting using a Breit−Wigner−Fano peak shape for the low-energy peak

* Address correspondence to richards@helios.phy.ohiou.edu.

Received for review June 23, 2011 and accepted August 11, 2011.

Published online August 11, 2011
10.1021/nn202327n

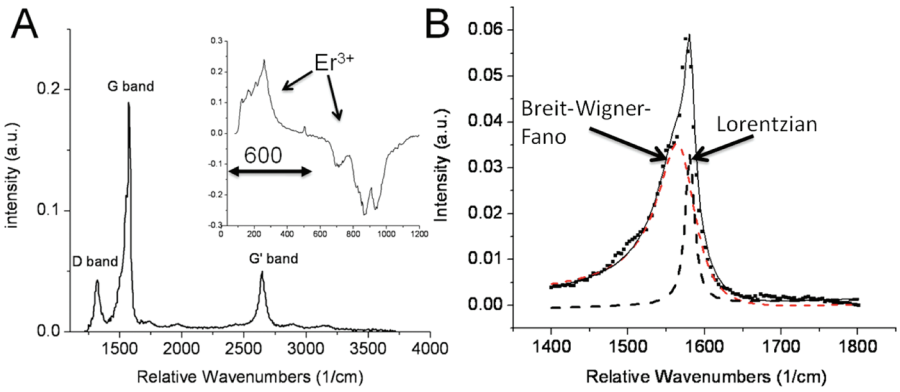

Figure 1. (A) SIMPLISMA spectra showing the spectral region of the SWCNT. The D, G, and G′ SWCNT bands are labeled in the figure. The inset zooms in on the spectral region where the Er^{3+} photoluminescence is observed. (B) Spectral region from the SWCNT G band. The red and black dotted lines are the fit of a Breit−Wigner−Fano and Lorentzian peaks, respectively, to the G band profile. The solid black line is the fit. The satisfactory fit shows that the SWCNT is metallic.

and a Lorentzian peak shape for the high-energy peak. The G band is shown in more detail in Figure 1B. The fitted peaks are shown as dotted lines, while the fit to the experimental data (solid squares) is the solid line in the figure. The Breit−Wigner−Fano peak shape is given by eq 1, where ω_{BWF} is the BWF frequency at maximum intensity I_o, $1/q$ is a parameter that measures the interaction of the phonon with the continuum, and Γ is the broadening parameter. From the fit, the Breit−Wigner−Fano peak yielded ω_{BWF} as 1570 cm^{-1}, Γ as 30 cm^{-1}, and $1/q$ as −0.2. The Lorentzian peak has a peak maximum and width (fwhm) of 1581 and 14 cm^{-1}, respectively. The Breit−Wigner−Fano peak shape and the fwhm of the Lorentzian peak are consistent with a metallic SWCNT. Metallic SWCNTs that have a diameter around 1 nm with a band gap around 2.33 eV are either 7,7 armchair metallic or 10,4 semimetal nanotubes.

$$I(\omega) = I_o \frac{[1+(\omega - \omega_{BWF})/q\Gamma]^2}{1+[(\omega - \omega_{BWF})/\Gamma]^2} \quad (1)$$

Thermal Behavior. A Raman scattering image of a SWCNT is shown in the left panel of Figure 2. The image is created by plotting the G band area at each pixel location. The temperature image (created from the relative photoluminescence Er^{3+} peaks) is shown in the right panel of Figure 2. The laser intensity is 8×10^{10} W/m^2, and the polarization of the excitation laser is aligned along the nanotube axis. The laser spot size is ∼400 nm. The temperature profiles taken parallel and perpendicular to the CNT are shown in Figure 3. The temperature profile perpendicular to the nanotube can be fitted with a Gaussian peak profile that has a fwhm of ∼300 nm. The maximum temperature change is 4.3 ± 0.2 K.

Figure 4 contrasts the temperature profile along the SWCNT when the excitation polarization is changed from parallel to perpendicular of the SWCNT axis. For perpendicular excitation, the temperature maximum located in the middle of the nanotube is diminished by a factor of 4 when compared to parallel excitation.

DISCUSSION

Model of Heat Transfer. The temperature profile along the SWCNT can be modeled using eq 2, where x is the direction along the wire, k_{wire} is the thermal conductivity of the nanowire, $\dot{q}$ is the heat generation per unit volume, A is the cross sectional area of the wire, h is the thermal transfer coefficient for heat dissipation into the substrate, and P is the perimeter at x under the wire in contact with the substrate. In this model, the heat only dissipates into the substrate and not through air.

$$-k_{wire}A\frac{dT}{dx} + \dot{q}Adx + hP(\Delta T)dx = -k_{wire}A\frac{dT}{dx} - k_{wire}A\left(\frac{d^2T}{dx^2}\right)dx \quad (2)$$

When the wire is excited in the middle and the temperature is measured at that point, heat can propagate in both directions to either end of the wire. The magnitude of heat dissipation increases with the temperature gradient between the SWCNT and the substrate. The term of eq 2 that models heat dissipation into the substrate is $hP(\Delta T)dx$. At steady state, the heat generation term, $\int \dot{q}Adx' = \int (C_{abs}I(x'))/(V_{exc})Adx'$, and the heat dissipation term, 12.8 $\int hP(\Delta T)dx$, are equal. The variable x' refers to the distance along the SWCNT that is excited with the laser light. In the heat generation term, the laser intensity is not constant over the SWCNT but varies as a Gaussian profile along the wire. We approximate the laser intensity in the direction of the wire as a constant average intensity using the average intensity of the laser over the length of SWCNT (300 nm). The average laser intensity is 7×10^{10} W/m^2 with a peak intensity of 8×10^{10} W/m^2. The factor 12.8 in the heat dissipation term relates the local temperature of the nanowire to the measured temperature.[25] This factor takes into account that our optical temperature measurement is resolution-limited and needs to be convoluted with the true thermal image in the substrate and the collection volume of our microscope.

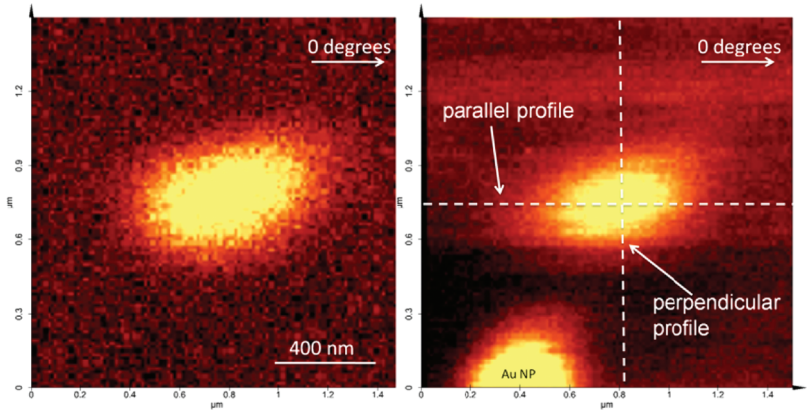

Figure 2. Left panel: Raman scattering image of a SWCNT. The excitation polarization is along the SWCNT axis. Right panel: Temperature image of a SWCNT constructed from the relative intensities in the photoluminescence of Er ions embedded in the thermal sensor film.

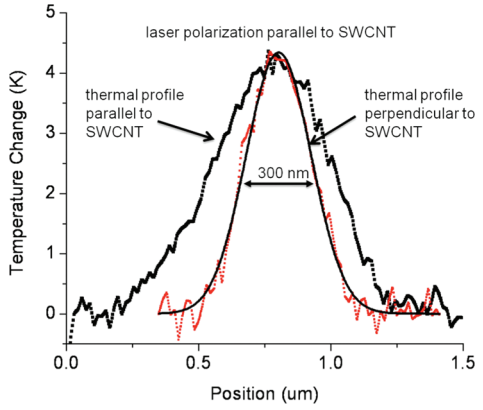

Figure 3. Temperature profile taken parallel and perpendicular to the SWCNT axis (shown as dotted lines) with laser polarization parallel to the SWCNT. The temperature profile perpendicular to the SWCNT axis is fitted with a Gaussian line shape that has a fwhm of ~300 nm.

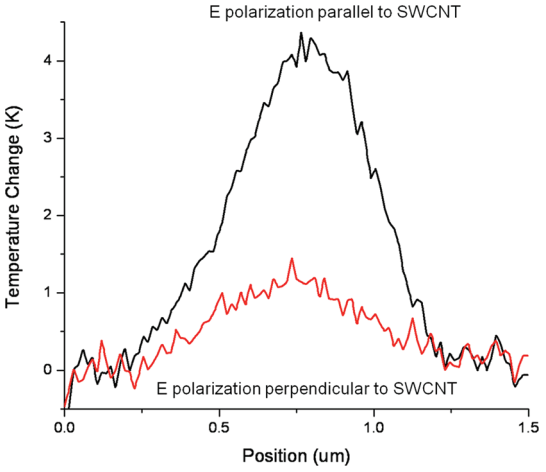

Figure 4. Temperature profile taken parallel to the SWCNT with laser polarization parallel and perpendicular to the SWCNT axis.

Equation 2 can be recast into eq 3 and solved using the appropriate boundary conditions.

$$\frac{d^2\theta}{dx^2} + \frac{hP}{k_{wire}A}\theta = 0 \qquad (3)$$

In this equation, temperature is transformed into θ where $\theta = T - T_\infty + (\dot{q}/k_{wire})$. The solution of this differential equation is $\theta = C_1 \exp(-mx) + C_2 \exp(mx)$, where $m^2 = (hP)/(k_{wire}A)$. After applying appropriate boundary conditions, the solution is $\theta/\theta_o = (\cosh(m(L - x)))/(\cosh(mL))$, where θ_o is θ at $x = 0$ and L is the length of the SWCNT. Finally, once the form of the temperature profile in the SWCNT is known, then energy balance can be used to solve for the temperature along the wire.

The thermal profile along the SWCNT axis when excited in the middle of the SWCNT is shown in Figure 5 as the blue dotted line. The thermal conductivity of the SWCNT is believed to be in excess of 3000 W/m·K.[3,28] This unusually high thermal conductivity leads to a nearly uniform temperature distribution along the SWCNT axis when the SWCNT is excited in the middle. If the thermal profile is constant, then the dissipation rate from the SWCNT is constant and does not depend upon the position along the SWCNT. The heat source then can be treated as a point source within a spherically symmetric coordinate system. This approximation will break down if the temperature profile along the SWCNT changes and the dissipation rate becomes a function of length along the SWCNT.

Absorption Cross Section. At steady state, the rate of heat generation and heat dissipation must be equal. In our case, the heat generator is the optically excited SWCNT, while the heat dissipation occurs only into the thermal sensor film. We can use this principle to determine the absorption cross section by measuring the local temperature of the film and realizing that the temperature decreases as $1/R$ away from a heat source in a spherically symmetric system. The absorption cross section at 532 nm excitation (C_{abs}^{NT}) is determined from the local temperature changed using eq 4 where R_e^{NT} is the effective radius of the SWCNT (R_e^{NT} = 3.83 nm), equal to $R_e^{NT} = ((3r^2l)/4))^{1/3}$, where r is the nanotube radius

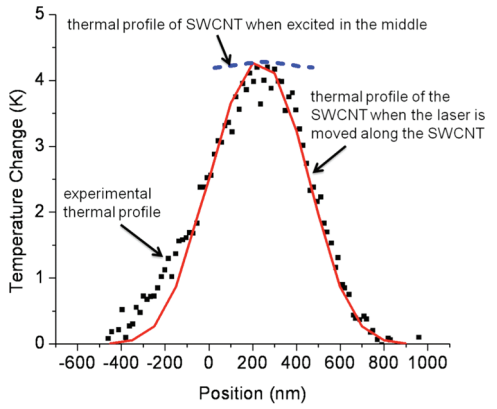

Figure 5. Temperature change in the thermal sensor film in close proximity to the SWCNT. Thermal profile is taken along the SWCNT axis for excitation polarization parallel and perpendicular to the SWCNT axis.

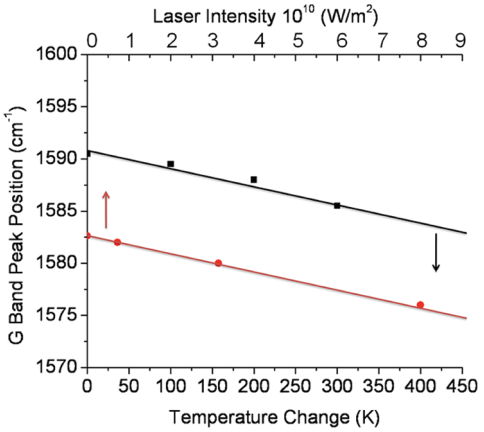

Figure 6. Black squares are for data taken from ref 29, where the G band peak position is plotted as a function of temperature. The temperature plotted on the lower *x* axis is relative to room temperature (300 K). The red circles are our data where the G band peak position has been determined as a function of laser intensity. The laser intensity is plotted on the upper *x* axis.

(0.5 nm), l is the nanotubes length (300 nm), k_o is the effective thermal conductivity of the film (0.75 W/m·K), and $\langle I \rangle$ is the average laser intensity over the SWCNT of 7×10^{10} W/m^2. The effective thermal conductivity (0.75 W/m·K) is only half the thermal conductivity of the film (1.5 W/m·K) because only half of the sphere is used to dissipate the heat away from the heat generator.[25]

$$\Delta T_{max} = \frac{C_{abs}^{NT}\langle I \rangle}{4\pi k_o R_e^{NT}} \quad (4)$$

The measured temperature of the thermal sensor film is appropriately scaled to give the local temperature as $\Delta T_{max} = 4.3 \times 12.8 = 55$ K, where the factor 12.8 is the optical transfer parameter that relates the measured diffraction-limited temperature to the local non-resolution-limited temperature.[25] The absorption cross section for an excitation polarization parallel to the SWCNT is 2.8×10^{-17} m^2 or 9.4×10^{-17} m^2/μm. This value is in reasonable agreement with other absorption cross section measurements for SWCNTs.[24] Figure 4 contrasts the temperature profile when the nanotube is excited using polarization parallel and perpendicular to the nanotube. The maximum temperature when exciting with perpendicular polarization is ~1/4 the maximum temperature if parallel polarization is used. Using this factor yields an absorption cross section of the SWCNT for perpendicular polarization of 7×10^{-18} m^2 or 2.4×10^{-17}m^2/ μm.

Once the absorption cross section is known, then the thermal transfer coefficient in eq 2 can be solved. Using an absorption cross section of 2.8×10^{-17} m^2 gives a value of 8×10^7 W/m^2·K for the thermal transfer coefficient. Equation 2 can now be used to generate the predicted thermal profile when the laser is moved along the SWCNT axis. The predicted thermal profile is shown as the solid red line in Figure 5. This profile reflects the Gaussian excitation profile of the laser because the SWCNT attains a uniform temperature profile at all laser excitations along the SWCNT axis. The temperature variation along the SWCNT axis comes about because of laser intensity changes instead of changes in the thermal profile along the axis.

Interfacial Thermal Conductance. The interfacial thermal conductance from the SWCNT to the thermal sensor film can be determined using eq 5, where j_Q is the heat flux across the interface, G is the interfacial conductance, and ΔT is the temperature difference at the interface between the SWCNT and the thermal sensor film.

$$j_Q = G\Delta T \quad (5)$$

The heat flux is determined from the absorption cross section for SWCNT,[23] and the size of the nanotube using $j_Q = (C_{abs}^{NT}\langle I \rangle)/(2\pi rl)$, where C_{abs}^{NT} is the absorption cross section (2.8×10^{-17} m^2), $\langle I \rangle$ is the average laser intensity (7×10^{10} W/m^2), and r and l are the radius and length of the nanotube.

We can determine the temperature of the SWCNT by observing the shift in frequency of the SWCNT G band with laser intensity. The position of the G band maximum has been shown to be temperature-dependent.[29] In Figure 6, we show the measured G band peak position as a function of laser intensity mapped onto peak position changes due to temperature.[29] The black squares, from previously published data,[29] show how the G band peak position changes with temperature while the red circles are our experimental data as a function of laser intensity. The linear trend in the data has identical slopes but different intercepts. The different intercepts are attributed to differences in the SWCNT. Even though the intercepts are different, the slope gives a good representation of the temperature-dependent G band spectral shift. The SWCNT temperature change (relative to room temperature) at

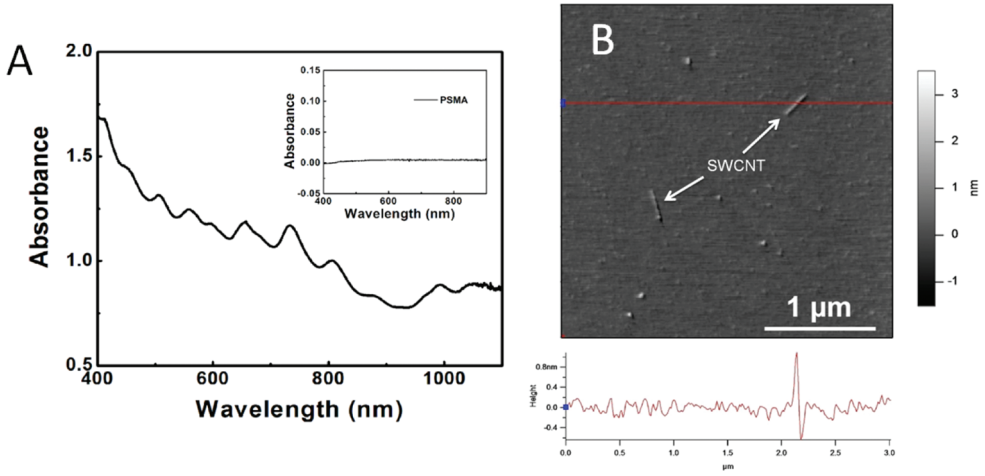

Figure 7. (A) UV−visible absorption spectrum of SWCNT suspension. Inset: UV−visible absorption spectrum of PSMA solution without SWCNTs. (B) AFM image of representative SWCNT on Si substrate. The diameter of the SWCNT is 1 nm with a length of 300 nm. Reprinted from ref 26, with permission from Elsevier.

our laser intensity of 7×10^{10} W/m^2 is ~370 K. Recalling that the local temperature of the thermal sensor film is 55 K, this gives a temperature difference (ΔT) between the SWCNT and the thermal sensor film of 315 K (370 K − 55 K = 315 K). From eq 5, we determine the interfacial thermal conductance (G) of 6.6 MW/m^2·K for a SWCNT. This value can be compared to previous measurements for the interfacial thermal conductance of SWCNT in octane suspensions of 12 MW/m^2·K.[18] The mechanism postulated for heat transfer from a nanotube to the octane liquid involves a bottleneck of energy transfer where high-frequency carbon nanotube phonon modes must be transferred to low-frequency modes through phonon−phonon coupling and then exchanged with the surrounding medium.[18] If this is indeed the mechanism and the rate-limiting step is the phonon mode conversion within the carbon nanotube, then the interfacial thermal conductance should be reasonably invariant to the surrounding medium and a value of ~7 MW/m^2·K for the SWCNT on an amorphous $Al_{0.94}Ga_{0.06}N$ surface is reasonable.

CONCLUSIONS

The heat generation and dissipation of an individual optically excited metallic single-walled carbon nanotube is characterized using a thermal sensor thin film of $Al_{0.94}Ga_{0.06}N$ embedded with Er^{3+}. A maximum of 4.3 K of temperature change is observed in the middle of the SWCNT when the SWCNT is excited with parallel polarization with an average intensity of 7×10^{10} W/m^2. From this temperature measurement, we deduce an absorption cross section for the SWCNT of 9.4×10^{-17} m^2/μm using parallel polarization and 2.4×10^{-17} m^2/μm for perpendicular polarization. The SWCNT G band shifts with laser intensity, and by mapping this shift on previous published temperature-dependent Raman spectra for SWCNT,[29] we measure a temperature difference between the SWCNT and the substrate of 315 K. This yields a value for the thermal interfacial conductance of 6.6 MW/m^2·K.

MATERIALS AND METHODS

Materials. HiPCO SWCNT powders were purchased from Carbon Nanotechnologies, Inc. (Houston,TX). Poly(styrene maleic anhydride) (PSMA, MW = 1600) was received from Polysciences, Inc. Dialysis tubing (12 000−14 000 Da molecular weight cutoff) was obtained from Spectrum Laboratories, Inc. Sodium hydroxide was purchased from Fisher Scientific.

SWCNT Suspension Preparation. To disperse SWCNTs, 1 mg of PSMA was dissolved in 2 mL of 0.1 M NaOH solution in a test tube, and ~1 mg of HiPCO SWCNTs was added in the polymer solution. The mixture was then sonicated for 30 min in an ice−water bath at a power level of 130 W, followed by 1 h centrifugation at 25 000g to obtain a SWCNT suspension in the supernatant. The supernatant was then dialyzed in deionized water (18.2 MΩcm, Millipore) for 1 day using molecular porous membrane dialysis tubing to remove free PSMA. The used dialysis solution was replaced with fresh deionized water every 6 h. The resulting SWCNT suspension was stable for weeks with no precipitation.

Absorption Spectrum of SWCNT Suspension. Absorption spectrum was measured by an Agilent 8453 UV−visible spectrophotometer. Absorption spectrum (see Figure 7A for representative spectrum) showed peaks in spectral range for the first interband transitions for metallic SWCNTs, M_{11} (400−600 nm), and the second interband transitions for semiconducting SWCNTs, S_{22} (550−900 nm).[8−10] The sharp peaks, due to van Hove transitions, indicate that the suspension is a well-dispersed mixture of metallic and semiconducting SWCNTs. As a comparison, the PSMA solution without SWCNTs showed a featureless absorption spectrum in the spectral range (Figure 7A, inset).

Atomic Force Microscopy (AFM) Characterization of SWCNT Suspension. Ten microliters of a SWCNT suspension was spin-coated onto a piece of Si substrate. The sample was then imaged at room temperature and ambient conditions using an MFP3D atomic force microscope (Asylum Research, Santa Barbara, CA) in AC mode (see Figure 7B). Probes with resonance frequency around 325 kHz (NSC15/AIBS, MikroMasch USA, Wilsonville, OR) were

used in imaging. The AFM image showed that SWCNTs were individually dispersed with around 1 nm diameter and several hundred nanometer length.[26]

Raman Imaging Microscope and Thermal Sensor Film. We use a scanning optical microscope imaging system (Witec α-SNOM) to collect confocal Raman and photoluminescence spectra that can be converted into images. Our procedure for collecting Raman spectra for the SWCNTs has been discussed in detail[26] as well as the characterization and properties of the thermal sensor film.[25] Only a brief description will be given here. The thermal sensor consists of a thin film (~270 nm thick) of amorphous $Al_{0.94}Ga_{0.06}N$ embedded with Er^{3+} ions on a silicon substrate.[30,31] The Er^{3+} ions are excited with 2.33 eV (532 nm) laser light resulting in a typical Er^{3+} photoluminescence spectrum. The relative intensities of the $^2H_{11/2} \rightarrow {}^4I_{15/2}$ and the $^4S_{3/2} \rightarrow {}^4I_{15/2}$ energy transitions of the Er^{3+} ions are temperature-dependent[30,32] and are related by a Boltzmann factor, $\exp(-\Delta E/kT)$, where ΔE is the energy difference between the two levels, k is the Boltzmann constant, and T is the absolute temperature. We use this relationship to convert Er^{3+} photoluminescence spectra to temperature.

Acknowledgment. This work was supported by a grant from the Biomimetic Nanoscience and Nanotechnology Initiative at Ohio University.

REFERENCES AND NOTES

1. Odom, T. W.; Huang, J. L.; Kim, P.; Lieber, C. M. Atomic Structure and Electronic Properties of Single-Walled Carbon Nanotubes. *Nature* **1998**, *391*, 62–64.
2. Hone, J.; Whitney, M.; Piskoti, C.; Zettl, A. Thermal Conductivity of Single-Walled Carbon Nanotubes. *Phys. Rev. B* **1999**, *59*, R2514–R2516.
3. Berber, S.; Kwon, Y. K.; Tomanek, D. Unusually High Thermal Conductivity of Carbon Nanotubes. *Phys. Rev. Lett.* **2000**, *84*, 4613–4616.
4. Pop, E.; Mann, D.; Wang, Q.; Goodson, K.; Dai, H. J. Thermal Conductance of an Individual Single-Wall Carbon Nanotube above Room Temperature. *Nano Lett.* **2006**, *6*, 96–100.
5. Xu, Z. P.; Buehler, M. J. Strain Controlled Thermomutability of Single-Walled Carbon Nanotubes. *Nanotechnology* **2009**, 20.
6. Treacy, M. M. J.; Ebbesen, T. W.; Gibson, J. M. Exceptionally High Young's Modulus Observed for Individual Carbon Nanotubes. *Nature* **1996**, *381*, 678–680.
7. Yang, Z. P.; Ci, L. J.; Bur, J. A.; Lin, S. Y.; Ajayan, P. M. Experimental Observation of an Extremely Dark Material Made by a Low-Density Nanotube Array. *Nano Lett.* **2008**, *8*, 446–451.
8. Bachilo, S. M.; Strano, M. S.; Kittrell, C.; Hauge, R. H.; Smalley, R. E.; Weisman, R. B. Structure-Assigned Optical Spectra of Single-Walled Carbon Nanotubes. *Science* **2002**, *298*, 2361–2366.
9. O'Connell, M. J.; Bachilo, S. M.; Huffman, C. B.; Moore, V. C.; Strano, M. S.; Haroz, E. H.; Rialon, K. L.; Boul, P. J.; Noon, W. H.; Kittrell, C.; *et al.* Band Gap Fluorescence from Individual Single-Walled Carbon Nanotubes. *Science* **2002**, *297*, 593–596.
10. Strano, M. S.; Dyke, C. A.; Usrey, M. L.; Barone, P. W.; Allen, M. J.; Shan, H. W.; Kittrell, C.; Hauge, R. H.; Tour, J. M.; Smalley, R. E. Electronic Structure Control of Single-Walled Carbon Nanotube Functionalization. *Science* **2003**, *301*, 1519–1522.
11. Yu, A. P.; Itkis, M. E.; Bekyarova, E.; Haddon, R. C. Effect of Single-Walled Carbon Nanotube Purity on the Thermal Conductivity of Carbon Nanotube-Based Composites. *Appl. Phys. Lett.* **2006**, *89*, 133102.
12. Kordas, K.; Toth, G.; Moilanen, P.; Kumpumaki, M.; Vahakangas, J.; Uusimaki, A.; Vajtai, R.; Ajayan, P. M. Chip Cooling with Integrated Carbon Nanotube Microfin Architectures. *Appl. Phys. Lett.* **2007**, *90*, 123105.
13. Hu, X. J.; Padilla, A. A.; Xu, J.; Fisher, T. S.; Goodson, K. E. 3-Omega Measurements of Vertically Oriented Carbon Nanotubes on Silicon. *J. Heat Transfer* **2006**, *128*, 1109–1113.
14. Chen, Z.; Wu, Z. Y.; Tong, L. M.; Pan, H. P.; Liu, Z. F. Simultaneous Dielectrophoretic Separation and Assembly of Single-Walled Carbon Nanotubes on Multigap Nanoelectrodes and Their Thermal Sensing Properties. *Anal. Chem.* **2006**, *78*, 8069–8075.
15. Krishna, V.; Stevens, N.; Koopman, B.; Moudgil, B. Optical Heating and Rapid Transformation of Functionalized Fullerenes. *Nat. Nanotechnol.* **2010**, *5*, 330–334.
16. De La Zerda, A.; Zavaleta, C.; Keren, S.; Vaithilingam, S.; Bodapati, S.; Liu, Z.; Levi, J.; Smith, B. R.; Ma, T. J.; Oralkan, O.; *et al.* Carbon Nanotubes as Photoacoustic Molecular Imaging Agents in Living Mice. *Nat. Nanotechnol.* **2008**, *3*, 557–562.
17. Chang, C. W.; Okawa, D.; Garcia, H.; Majumdar, A.; Zettl, A. Nanotube Phonon Waveguide. *Phys. Rev. Lett.* **2007**, *99*, 045901.
18. Huxtable, S. T.; Cahill, D. G.; Shenogin, S.; Xue, L. P.; Ozisik, R.; Barone, P.; Usrey, M.; Strano, M. S.; Siddons, G.; Shim, M.; *et al.* Interfacial Heat Flow in Carbon Nanotube Suspensions. *Nat. Mater.* **2003**, *2*, 731–734.
19. Shenogin, S.; Xue, L. P.; Ozisik, R.; Keblinski, P.; Cahill, D. G. Role of Thermal Boundary Resistance on the Heat Flow in Carbon-Nanotube Composites. *J. Appl. Phys.* **2004**, *95*, 8136–8144.
20. Bui, K.; Duong, H. M.; Striolo, A.; Papavassiliou, D. V. Effective Heat Transfer Properties of Graphene Sheet Nanocomposites and Comparison to Carbon Nanotube Nanocomposites. *J. Phys. Chem. C* **2011**, *115*, 3872–3880.
21. Teng, C. C.; Ma, C. C. M.; Chiou, K. C.; Lee, T. M.; Shih, Y. F. Synergetic Effect of Hybrid Boron Nitride and Multi-walled Carbon Nanotubes on the Thermal Conductivity of Epoxy Composites. *Mater. Chem. Phys.* **2011**, *126*, 722–728.
22. Fujii, M.; Zhang, X.; Xie, H. Q.; Ago, H.; Takahashi, K.; Ikuta, T.; Abe, H.; Shimizu, T. Measuring the Thermal Conductivity of a Single Carbon Nanotube. *Phys. Rev. Lett.* **2005**, *95*, 065502.
23. Islam, M. F.; Milkie, D. E.; Kane, C. L.; Yodh, A. G.; Kikkawa, J. M. Direct Measurement of the Polarized Optical Absorption Cross Section of Single-Wall Carbon Nanotubes. *Phys. Rev. Lett.* **2004**, *93*, 037404.
24. Berciaud, S.; Cognet, L.; Lounis, B. Luminescence Decay and the Absorption Cross Section of Individual Single-Walled Carbon Nanotubes. *Phys. Rev. Lett.* **2008**, *101*, 077402.
25. Carlson, M. T.; Khan, A.; Richardson, H. H. Local Temperature Determination of Optically Excited Nanoparticles and Nanodots. *Nano Lett.* **2011**, *11*, 1061–1069.
26. Richardson, H. H.; Wang, D. Spatial Enhancement of Raman Scattering Images Using Moving-Window Two-Dimensional Auto-correlation Spectroscopy. *J. Mol. Struct.* **2010**, *974*, 52–55.
27. Windig, W.; Stephenson, D. A. Self-Modeling Mixture Analysis of 2nd-Derivative Near-Infrared Spectral Data Using the Simplisma Approach. *Anal. Chem.* **1992**, *64*, 2735–2742.
28. Kim, P.; Shi, L.; Majumdar, A.; McEuen, P. L. Thermal Transport Measurements of Individual Multiwalled Nanotubes. *Phys. Rev. Lett.* **2001**, *87*, 215502.
29. Zhou, Z. P.; Dou, X. Y.; Ci, L. J.; Song, L.; Liu, D. F.; Gao, Y.; Wang, J. X.; Liu, L. F.; Zhou, W. Y.; Xie, S. S.; *et al.* Temperature Dependence of the Raman Spectra of Individual Carbon Nanotubes. *J. Phys. Chem. B* **2006**, *110*, 1206–1209.
30. Gurumurugan, K.; Chen, H.; Harp, G. R.; Jadwisienczak, W. M.; Lozykowski, H. J. Visible Cathodoluminescence of Er-Doped Amorphous Aln Thin Films. *Appl. Phys. Lett.* **1999**, *74*, 3008–3010.
31. Dimitrova, V. I.; Van Patten, P. G.; Richardson, H.; Kordesch, M. E. Photo-, Cathodo-, and Electroluminescence Studies of Sputter Deposited Aln: Er Thin Films. *Appl. Surf. Sci.* **2001**, *175*, 480–483.
32. Garter, M. J.; Steckl, A. J. Temperature Behavior of Visible and Infrared Electroluminescent Devices Fabricated on Erbium-Doped Gan. *IEEE Trans. Electron Devices* **2002**, *49*, 48–54.